ACS Energy LETTERS

http://pubs.acs.org/journal/aelccp

Multifunctional Photovoltaic Window Layers for Solar-Driven Catalytic Conversion of CO_2: The Case of CIGS Solar Cells

Julian Guerrero, Elisabeth Bajard, Nathanaelle Schneider, Fabienne Dumoulin, Daniel Lincot, Umit Isci,* Marc Robert,* and Negar Naghavi*

Cite This: *ACS Energy Lett.* 2023, 8, 3488−3493

Read Online

ACCESS | Metrics & More | Article Recommendations | Supporting Information

ABSTRACT: **Using a fast and simple one-step electrochemical method, we developed transparent and conductive ZnO nanoporous layers encapsulating molecular catalysts, showcasing dual functionality as a window layer for thin-film solar cells and a catalytic layer for solar-to-fuel conversion. As a proof of concept, tetraammonium-substituted Co phthalocyanine (CoPcTA) was encapsulated into the window layer of high-efficiency Cu(In,Ga)Se_2 (CIGS) solar cells demonstrating photoelectrochemical (PEC) reduction of CO_2 into CO with a selectivity of 93% and current densities up to ca. 7 mA cm^{-2} at −1.7 V vs SCE under 1 sun irradiation, which corresponds to a turnover number (TON) of above 100000 and a turnover frequency (TOF) of 10 s^{-1} after 3 h. The simplicity and versatility of this approach make the nanoporous catalytic ZnO layer not only easily adaptable to different high-efficiency solar cells but also pave the way for flexible testing of diverse molecular catalysts for CO_2 conversion into diverse, valuable fuels.**

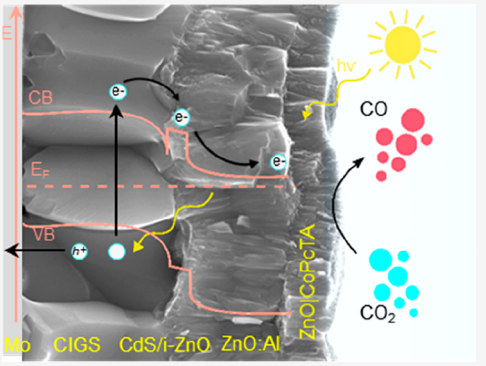

Photovoltaics (PV) are currently one of the fastest-growing renewable industries. In this context, driving catalytic chemical reactions from PV using photoelectrochemical (PEC) approaches offers a sustainable means of synthesizing chemicals and fuels while enabling the storage of intermittent solar energy. Efficient PV and solar-to-fuel technologies rely on semiconducting materials capable of converting sunlight to either direct current electricity or chemicals. In both cases, the efficiency depends on the ability of the material to absorb light and generate charge carriers. The absorbers used for photovoltaic applications are excellent candidates as photoelectrodes, presenting a high photocurrent due to their ability to absorb the major part of visible light. However, these materials alone often lack sufficient energy to trigger the CO_2 reduction reaction (CO_2RR) and require high bias voltages or coupling with other materials.

In photovoltaics, the mechanism for charge carrier separation, based on the pn-junction, generally outperforms the solid−liquid analogue in terms of charge separation and electron transport.

In the electrochemical CO_2RR, efficient catalysts are needed to facilitate multiple electron and proton transfers, achieving high current densities and selectivity. Molecular catalysis is very promising, as atom-efficient catalysts with high intrinsic activities and tunable active sites are used.[1,2] Such catalysts, with easily identifiable and tunable active sites, offer a variety of options for controlling the activity and product selectivity.[1]

Encapsulating molecular catalysts directly within the window layers of PV solar cells, rather than grafting them onto additional layers like TiO_2,[3−8] is an appealing approach. This eliminates the need for chemical modifications of catalysts and complex deposition processes and simplifies manufacturing. The development of a transparent and conducting layer integrating efficient catalysts as a window layer on different PV solar cells holds numerous advantages, including enhanced performance, higher efficiency for charge transport to catalytic sites, and better stability due to lower catalyst leaching, leading to the development of a better-performing photocathode.

Most standard solar cells end up at their front side by a transparent and conducting layer, such as ZnO:Al, In_2O_3:Sn (ITO), or SnO_2:F (FTO), called a window layer.[9−12] This paper discusses the development of a transparent and

Received: June 18, 2023
Accepted: July 21, 2023
Published: July 24, 2023

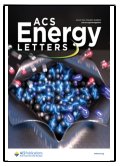

https://doi.org/10.1021/acsenergylett.3c01205
ACS Energy Lett. 2023, 8, 3488−3493

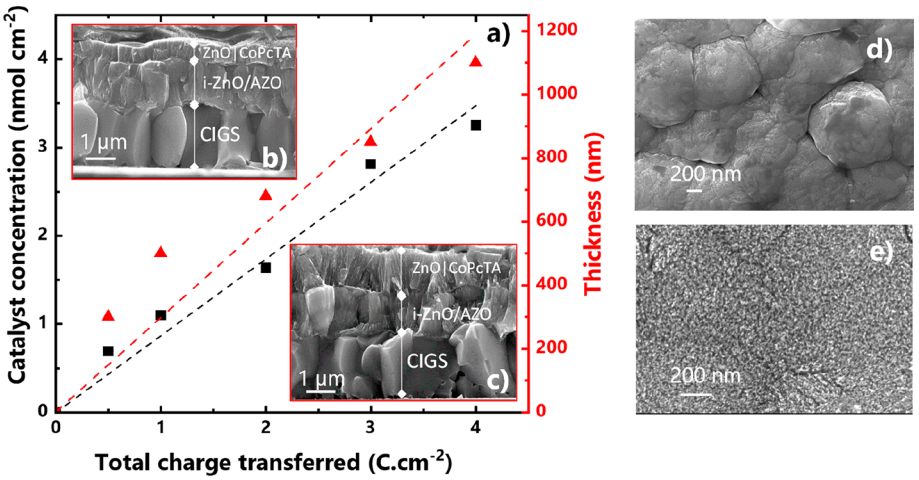

Figure 1. (a) ZnO|CoPcTA NP layer thickness (as determined from SEM images, red triangles) and CoPcTA concentration (in nmol cm^{-2}, quantified by ICP analysis, black squares) as a function of the total charge transferred during electrodeposition (in C cm^{-2}). (b, c) Cross-section SEM images of the modified Mo/CIGS/CdS/i-ZnO/ZnO:Al electrodes upon adding ZnO|CoPcTA NP layers of 500 and 1100 nm, respectively. (d, e) Top view SEM images of the Mo/CIGS/CdS/i-ZnO/ZnO:Al electrodes before and after addition of the ZnO|CoPcTA NP layer, respectively.

conductive nanoporous ZnO layer encapsulating a molecular catalyst for use as a front contact layer in Cu(In,Ga)Se_2 (CIGS) solar cells. CIGS is a promising PV thin film technology known for its high efficiency, stability, and low manufacturing cost. CIGS-based solar cells have achieved a record efficiency of 23.6%.[13] Because of its direct bandgap and high absorption coefficient (α = 10^7−10^8 m^{-1} in the visible region, Figure S1), the CIGS alloy is a high-performance absorber material where only 1−2 μm is required to absorb the maximum number of photons. In these solar cells, p-type polycrystalline CIGS is deposited on soda lime glass covered with molybdenum (Mo), forming a heterojunction with a CdS layer and an i/n-ZnO:Al front contact (Figure S2).

The nanoporous ZnO layer serves multiple functions, acting as a front contact and protective layer for the solar cell and adding catalytic activity to the CIGS photoelectrode for solar-to-fuel conversion. ZnO is chosen for its unique advantages, such as being easily prepared in high quality and in various structures and shapes[14−17] using solution routes like electrodeposition.[18,19] The solution environment promotes self-assembly structures, and the nanostructured architecture of ZnO facilitates the movement of electrons and holes due to quantum confinement.

In the optimization process, a standard CIGS cell absorber with a bandgap of 1.2 eV was used in a standard configuration of glass/Mo/CIGS/CdS/i-ZnO/ZnO:Al. A water-soluble tetracationic Co phthalocyanine complex (Figure S3) was encapsulated into the nanoporous ZnO layer during its photoelectrodeposition on the ZnO:Al window layer of the CIGS solar cells. The thickness of the ZnO|CoPcTA nanoporous (ZnO|CoPcTA NP) layer and the concentration of the catalyst could be controlled by adjusting the transferred charge during the ZnO growth process, as observed in Figure 1a.[20] Increasing the charge from 0 to 4 C cm^{-2} results in a relatively linear increase in the ZnO|CoPcTA NP thickness up to 1200 nm. SEM cross-section images of Mo/CIGS/CdS/i-ZnO/ZnO:Al/ZnO|CoPcTA NP cells (Figure 1b,c) reveal that the top nanoporous layer presents a fibrous internal nanostructure aligned in the direction of film growth, which is consistent with similar ZnO/organic layers developed in the literature.[18,21] The top-view SEM images confirm the change in morphology, with the ZnO|CoPcTA NP window layer exhibiting a spongelike porous surface compared to the dense sputtered ZnO thin film (Figure 1d,e). Inductively coupled plasma optical emission spectrometry (ICP-OES) on ZnO|CoPcTA NP samples confirmed the incorporation of the molecular catalyst into the electrodeposited layers. Measurements show that the concentration of the CoPcTA molecule in the layers is linearly correlated to the film thickness, and the catalyst concentration remains in the order of a nanomoles per square centimeter (from 0.5 to 3.6 nmol cm^{-2}, Figure 1a).

The ZnO|CoPcTA NP layers were subjected to detailed analysis using X-ray photoelectron spectroscopy (XPS, Figure S4), energy dispersive X-ray spectroscopy (EDX, Figure S5), Fourier transform infrared spectroscopy (FTIR, Figure S6), and atomic force microscopy (AFM, Figure S9). They confirmed that the CoPcTA catalyst is effectively incorporated and uniformly dispersed within the ZnO layer, without any observed aggregation of cobalt. Comparisons between the X-ray diffraction patterns of the sputtered-ZnO:Al substrate and the ZnO|CoPcTA NP layer (Figure S7) revealed that both layers exhibit a well-crystallized ZnO wurtzite type structure. The highly preferred orientation along the (002) direction confirms the internal crystalline quality of the layer, which can favor electron transport properties.

The impact of hybrid nanoporous layers on the performance of CIGS solar cells was evaluated through J−V measurements under 1 sun illumination (100 mW cm^{-2} AM 1.5G). The thickness of the ZnO|CoPcTA NP layer ranged from 0 to 1000 nm. The efficiency (η), fill factor (FF), open circuit voltage (V_{OC}), and short circuit current density (J_{SC}) of the solar cells were compared to those of a nonmodified CIGS solar cell (Table 1). Increasing the thickness of the ZnO|CoPcTA NP layers up to 1000 nm primarily affects the J_{SC} and FF of the cells. J_{SC} decreases from 33.9 to 27.2 mA cm^{-2}, and FF decreases from 75% to 67%, resulting in a slight decrease in V_{OC} from 698 to 633 mV. Consequently, the efficiency of the modified CIGS cells diminishes from 17.8% to 9.0% for ZnO|CoPcTA NP layer thicknesses up to 1000 nm. The diminution in FF can be attributed to the introduction of a new layer,

https://doi.org/10.1021/acsenergylett.3c01205
ACS Energy Lett. 2023, 8, 3488−3493

Table 1. $J-V$ Parameters of the Modified CIGS Cells

sample	J_{SC} (mA cm^{-2})	V_{OC} (mV)	FF (%)	η (%)
CIGS cell	33.9	698	75	17.8
CIGS cell + ZnO|CoPcTA NP 350 nm	31.4	685	71	15.8
CIGS cell + ZnO|CoPcTA NP 600 nm	29.3	663	67	12.1
CIGS cell + ZnO|CoPcTA NP 1000 nm	27.2	633	67	9.0

which creates additional interfaces, leading to losses in electron transport and recombination facilitation. The lower J_{SC} may be due to lower transmission of the ZnO|CoPcTA NP layers compared with standard ZnO:Al layers in the visible wavelength range. However, even with a 1000 nm thick nanoporous layer, current densities of up to 27 mA cm^{-2} can still be achieved. The external quantum efficiency (EQE) measurements (Figure 2) showed a decrease in the EQE

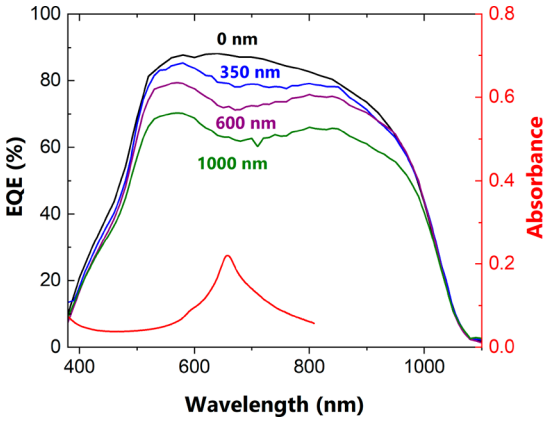

Figure 2. External quantum efficiency (EQE) of CIGS solar cells covered with ZnO|CoPcTA NP layers with thicknesses from 0 to 1000 nm compared with the absorption spectra of 50 μM CoPcTA molecules in aqueous solution.

curves, particularly in the wavelength region between 550 and 850 nm, as the thickness of the ZnO|CoPcTA NP layers increased. This corresponds to the absorbance region of the CoPcTA molecule, explaining the reduction in the number of electrons produced in that wavelength region.

To enable solar-to-fuel applications, the hybrid layer added to the CIGS device needs to be thin enough to allow light transmission while containing an adequate amount of catalyst for catalytic activity. After conducting several tests, a ZnO|CoPcTA NP layer with a thickness of 350 nm was selected for subsequent experiments, so as to favor high photovoltaic efficiency for PEC-CO_2 reduction while minimizing current losses.

To investigate the CO_2 reduction activity of the modified CIGS device under PEC conditions, linear sweep voltammetry (LSV) experiments were performed under chopped AM 1.5G illumination in a 0.1 M $TBAPF_6$ acetonitrile solution with 1% and 2% water as proton sources, saturated with either Ar or CO_2 (Figure 3a). The addition of a proton source was found to enhance the catalytic performance of the ZnO|CoPcTA NP layers,[20] most likely by accelerating CO_2 protonation and C–O bond cleavage[23−25] along with the overall reaction

$$CO_2 + H_2O + 2e^- \rightarrow CO + 2OH^- \quad (1)$$

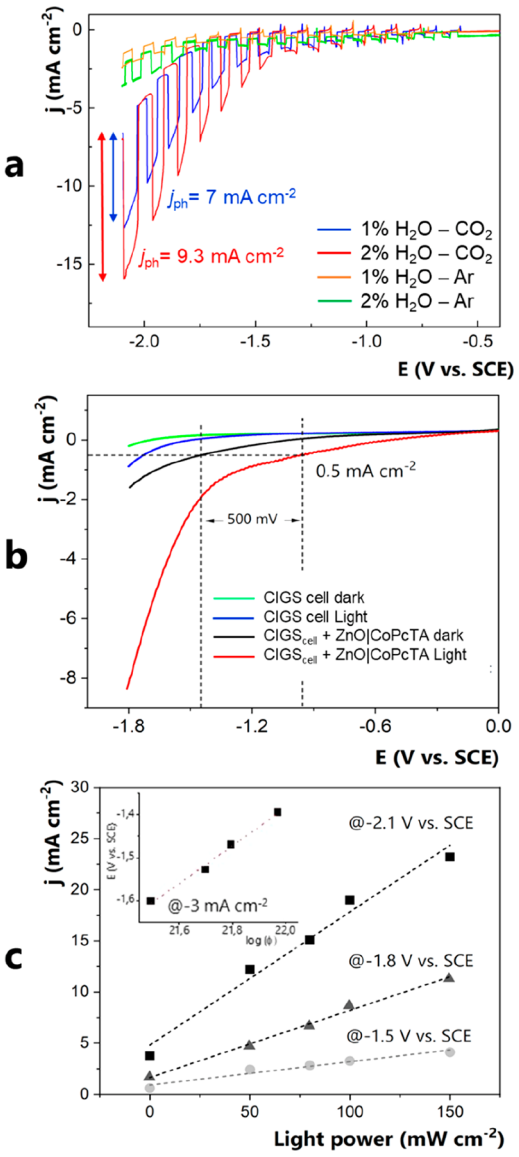

Figure 3. (a) Linear sweep voltammograms under chopped illumination (100 mW cm^{-2}) of a Mo/CIGS/CdS/i-ZnO/ZnO:Al + ZnO|CoPcTA NP (350 nm) photoelectrode under an Ar- or CO_2-saturated 0.1 M $TBAPF_6$ acetonitrile solution, with water concentrations ranging from 1 to 2%. The scan rate was 100 mV s^{-1}. (b) Linear sweep voltammograms of a Mo/CIGS/CdS/i-ZnO/ZnO:Al photoelectrode compared to a Mo/CIGS/CdS/i-ZnO/ZnO:Al + ZnO|CoPcTA NP (350 nm) photoelectrode in the dark and upon illumination (100 mW cm^{-2}) in a CO_2-saturated 0.1 M $TBAPF_6$ and 2% H_2O acetonitrile solution. The scan rate was 100 mV s^{-1}. (c) Current density as a function of the light power, measured at −2.1, −1.8, and −1.5 V vs SCE, respectively. Inset: potential applied to reach a current density of 3.0 mA cm^{-2} as a function of the incident flux (log Φ_0).

On Figure 3a, upon saturating the solution with argon, a small cathodic current is observed, attributed to the hydrogen evolution reaction, reaching around −2.4 mA cm^{-2} at −2.1 V vs SCE. Upon CO_2 saturation, a current density of ca. −12.5 mA cm^{-2} was measured at −2.1 V vs SCE, with a photogenerated current difference (j_{ph}) of up to 7 mA cm^{-2} between dark and illuminated current. Increasing the water concentration to 2% significantly enhanced the current density, reaching a maximum value of approximately −16.2 mA cm^{-2} at

https://doi.org/10.1021/acsenergylett.3c01205
ACS Energy Lett. 2023, 8, 3488−3493

−2.1 V vs SCE, with a photogenerated current of around −9.3 mA cm^{-2}. Further increasing the water concentration did not have a significant effect on the current density but promoted a higher production of hydrogen and faster degradation of the photoelectrode. The maximum current density achieved (−16.2 mA cm^{-2} at −2.1 V vs SCE) is higher than previously reported results in organic solvents[22] but lower than the expected performance based on the CIGS solar cell characteristics (J_{SC} ≈ 31 mA cm^{-2}) reported in Table 1. This lower photocurrent may be attributed to carrier recombination in different stages of the process.

In Figure 3b, the LSV of a CIGS solar cell (Mo/CIGS/CdS/i-ZnO/ZnO:Al) and a modified CIGS electrode with an additional ZnO|CoPcTA NP layer is compared in the dark and under illumination (100 mW cm^{-2}). The modified CIGS electrode reached a current density of −8.3 mA cm^{-2} at −1.8 V, compared to the nonmodified CIGS cell reaching −1.0 mA cm^{-2} at the same potential. This demonstrates the improved catalytic performance upon incorporation of a ZnO|CoPcTA NP layer. On the same curve, the illuminated Mo/CIGS/CdS/i-ZnO/ZnO:Al/ZnO|CoPcTA electrode achieved a current density of −0.5 mA cm^{-2} at a slightly negative potential of −0.95 V vs SCE. However, in the dark, the same current density required a high overpotential of −1.47 V vs SCE. Upon illumination, the Mo/CIGS/CdS/i-ZnO/ZnO:Al/ZnO|CoPcTA NP cathode presents a photovoltage of ca. 0.5 V, this value being slightly lower than the V_{OC} delivered by the CIGS solar cell (Table 1). Although a fraction of the incident light is absorbed by the ZnO|CoPcTA NP top layer of the solar cell, the majority of photons penetrate through the CIGS/CdS pn-junction. These photons generate electrons that are then transported to the catalytic centers of the hybrid layer. The higher photocurrents observed in Mo/CIGS/CdS/i-ZnO/ZnO:Al/ZnO|CoPcTA NP electrodes compared with standard CIGS solar cells demonstrate the improved catalytic performance of the system thanks to the incorporation of a layer of ZnO hybrid molecular catalyst on top of the CIGS solar cells.

To understand the relationship among photon flux, photocurrent, and photovoltage, we studied the impact of light power on photocurrent in the modified CIGS electrodes of the PEC CO_2 reduction system. Figure 3c displays the current density variation as the light power ranges from 0 to 150 mW cm^{-2}. In solar cells, the photocurrent (J_{tot}) is directly proportional to the absorbed photon flow (Φ_0): $J_{tot} \approx q\Phi_0$. Thus, the current density increases linearly with a higher light power intensity. Additionally, the inset to Figure 3c demonstrates that for a current density of −3 mA cm^{-2}, the potential is logarithmically proportional to the incident flux (Φ_0). This is the expected behavior of a solar cell under normal conditions, indicating that the modified device with the ZnO|CoPcTA NP layer maintains a strong photovoltaic response even after a light-assisted electrodeposition process. The linearity suggests that the electrocatalysis process is not limited by CO_2 or proton diffusion but rather by the absorbed photons converted into electron−hole pairs. Upon increasing the light power to 150 mW cm^{-2}, current densities of up to −22.7, −11.2, and −4.5 mA cm^{-2} at −2.1, −1.8, and −1.5 V vs SCE were respectively obtained.

The mechanism for CO_2 reduction over CIGS solar cells can be summarized as follows (Figure 4). On illumination, incoming photons generate electron−hole pairs within the CIGS absorbers. The pn-junction between CIGS and CdS facilitates the separation and collection of these charges. The

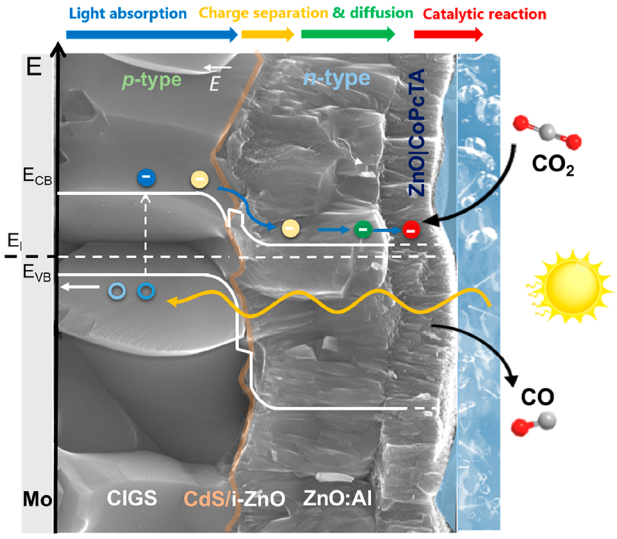

Figure 4. Schematic representation of a Mo/CIGS/CdS/i-ZnO/ZnO:Al photoelectrode covered with a ZnO|CoPcTA NP layer.

electric field across the pn-junction directs electrons from the p-type absorber to the n-type buffer layer and further transports them through the highly conducting ZnO:Al window layer. These electrons eventually reach the ZnO|CoPcTA NP layer, where they are directed to the incorporated molecular catalyst to facilitate the electrochemical CO_2 reduction reaction. However, increasing the thickness of the nanoporous layer, while increasing the quantity of catalysts, negatively impacts the J_{SC} and FF of the solar cells. Since a part of the electronic transport occurs between the ZnO nanopores, the catalysts, and the electrolyte, part of the photogenerated electrons may accumulate in the ZnO layer or be recombined at the ZnO/molecular catalysis interface.[26]

Figure 5a demonstrates the PEC CO_2 reduction under 100 mW cm^{-2} illumination using different electrode stacks: a standard CIGS solar cell, a CIGS solar cell with a hybrid ZnO|CoPcTA NP, and a pure CoPcTA molecule loaded on a carbon electrode. All chronoamperometry experiments were conducted at a constant potential of −1.5 V vs SCE for a minimum of 3 h. By adding a 350 nm thick nanoporous ZnO layer encapsulating only 0.75 nmol cm^{-2} of CoPcTA, the CIGS system achieves significant catalytic CO_2 reduction with 94% selectivity, sustaining high current densities of around −4 mA cm^{-2} for at least 3 h; H_2 was the only byproduct detected by gas chromatography (and as revealed by ^{1}H NMR studies of the liquid phase, no liquid products were formed). The incorporation of molecular catalysts enhances the photoelectrode's current densities, achieving 4 times higher values compared to a standard CIGS solar cell.

To evaluate the performance and stability of a photoelectrode under current densities higher than −4 mA cm^{-2}, a PEC-CO_2 reduction experiment was conducted at a current density of −7 mA cm^{-2} (Figure 5b) using the best electrolyte conditions: a CO_2-saturated 0.1 M $TBAPF_6$ and 2% H_2O acetonitrile solution. The high current density was sustained for 3 h. The initial potential value was approximately −1.55 V vs SCE, gradually shifting to around −1.70 V vs SCE. Under these conditions, the system consistently produced −7 mA cm^{-2} with an average CO selectivity of approximately 93%, corresponding to a partial current density for CO production (j_{CO}) of ca. −6.5 mA cm^{-2}, only obtaining 8% of H_2 as the

https://doi.org/10.1021/acsenergylett.3c01205
ACS Energy Lett. 2023, 8, 3488−3493

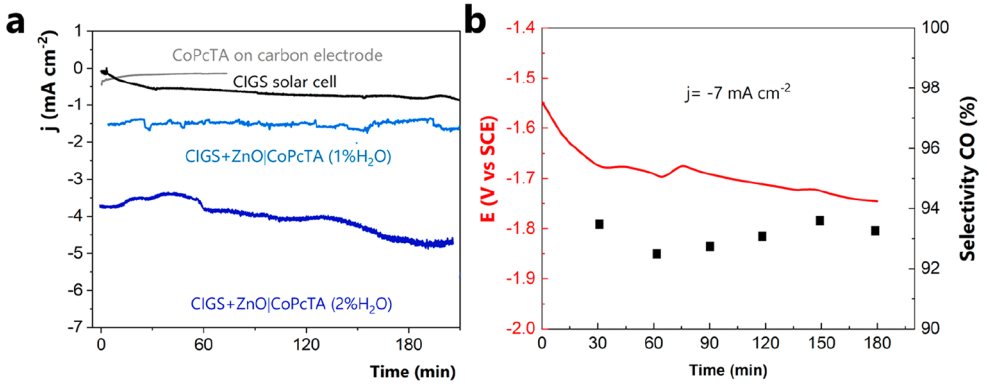

Figure 5. Chronoamperometry of CIGS photocathodes for PEC CO_2 reduction in CO_2-saturated 0.1 M $TBAPF_6$ acetonitrile solution. (a) Comparison of CO_2 electrolysis using CoPcTA loaded on carbon electrode with PEC-CO_2 reduction using a standard CIGS cell and a modified CIGS cell with a ZnO|CoPcTA NP (350 nm) window layer at −1.5 V vs SCE. (b) Potential of the electrode and selectivity for a constant current density held at −7 mA cm^{-2}, using a Mo/CIGS/CdS/i-ZnO/ZnO:Al + ZnO|CoPcTA NP (350 nm) photoelectrode adding 2% H_2O. Electrode surface: 0.5 cm^2. Light power: 100 mW cm^{-2}.

byproduct, a turnover number (TON) of above 100000, and a turnover frequency (TOF) of 10 s^{-1} (see the Supporting Information). Figure S9 demonstrates the long-term stability of a Mo/CIGS/CdS/i-ZnO/ZnO:Al + ZnO|CoPcTA photoelectrode (350 nm) during PEC-CO_2 reduction at an applied potential of −1.45 V vs SCE over 10 h. The current density of the photoelectrode remains relatively stable throughout the experiment, with a slight decrease from −1.6 to −1.27 mA cm^{-2}, and the CO selectivity is close to 92% throughout the entire experiment.

In summary, our study introduces a versatile functional window layer that encapsulates molecular catalysts, achieving high catalytic activity with minimal use of molecular materials and a straightforward preparation method. These functional window layers were easily integrated onto high-efficiency CIGS-based solar cells within only a few minutes using a light-assisted electrodeposition process. The resulting Mo/CIGS/CdS/i-ZnO/ZnO:Al/ZnO|CoPcTA NP stack presents a current density of up to −7 mA cm^{-2} at −1.7 V vs SCE for 3 h under visible light irradiation in an acetonitrile solution, with a CO selectivity of >92%. This remarkable performance can be attributed to the combined effects of the catalytic properties of the hybrid layer comprising ZnO and CoPcTA molecular catalyst, efficient light harvesting of the CIGS material, rapid charge transport within the CIGS cell layers, enabling electron transfer to the catalytic centers in the outermost layer, and swift CO_2 reduction at the catalytic sites. Furthermore, by slightly increasing the light intensity to 150 mW cm^{-2}, we achieved current densities of up to 22 mA cm^{-2} at −2.1 V vs SCE in an organic solvent, surpassing state-of-the-art PEC CO_2RR systems employing cocatalysts (Table T-S1). This approach offers versatility, as it can be applied to various high-efficiency solar cells, providing flexibility to test a large set of molecular catalysts without performing chemical modification. Additionally, it offers the potential for enhanced visible light absorption and improved catalytic efficiency of PEC systems.

■ ASSOCIATED CONTENT

Supporting Information

The Supporting Information is available free of charge at https://pubs.acs.org/doi/10.1021/acsenergylett.3c01205.

Experimental data to support the results of the main text (experimental details, XPS, EDX, ATR-IR, AFM, XRD, long-term PEC experiment, product quantification, and comparison among state-of-the-art photocathodes for PEC CO_2 reduction in various solvents) (PDF)

■ AUTHOR INFORMATION

Corresponding Authors

Umit Isci − *Marmara University, Faculty of Technology, Department of Metallurgical & Materials Engineering, 34722 Istanbul, Türkiye*; Email: umit.isci@marmara.edu.tr

Marc Robert − *Laboratoire d'Electrochimie Moléculaire, Université Paris Cité, CNRS, F-75013 Paris, France; Institut Universitaire de France (IUF), F-75005 Paris, France*; orcid.org/0000-0001-7042-4106; Email: robert@u-paris.fr

Negar Naghavi − *Institut Photovoltaïque d'Île-de-France (IPVF), CNRS, 91120 Palaiseau, France*; orcid.org/0000-0002-6045-5096; Email: negar.naghavi@chimieparistech.psl.eu

Authors

Julian Guerrero − *Laboratoire d'Electrochimie Moléculaire, Université Paris Cité, CNRS, F-75013 Paris, France; Institut Photovoltaïque d'Île-de-France (IPVF), CNRS, 91120 Palaiseau, France*

Elisabeth Bajard − *Institut Photovoltaïque d'Île-de-France (IPVF), CNRS, 91120 Palaiseau, France*

Nathanaelle Schneider − *Institut Photovoltaïque d'Île-de-France (IPVF), CNRS, 91120 Palaiseau, France*

Fabienne Dumoulin − *Acıbadem Mehmet Ali Aydınlar University, Faculty of Engineering and Natural Sciences, Biomedical Engineering Department, 34752 Istanbul, Türkiye*; orcid.org/0000-0002-0388-8338

Daniel Lincot − *Institut Photovoltaïque d'Île-de-France (IPVF), CNRS, 91120 Palaiseau, France*

Complete contact information is available at: https://pubs.acs.org/10.1021/acsenergylett.3c01205

Author Contributions

The manuscript was written through contributions of all authors. All authors have given approval to the final version of the manuscript.

https://doi.org/10.1021/acsenergylett.3c01205
ACS Energy Lett. 2023, 8, 3488−3493

Notes

The authors declare no competing financial interest.

■ ACKNOWLEDGMENTS

The authors are very grateful for the financial support from the CNRS through the 80|Prime program. M.R. acknowledges the Institut Universitaire de France (IUF) for partial financial support. The authors thank NICE Solar Energy GmbH for supplying the solar cells used in this work.

■ REFERENCES

(1) Dalle, K. E.; Warnan, J.; Leung, J. J.; Reuillard, B.; Karmel, I. S.; Reisner, E. Electro- and Solar-Driven Fuel Synthesis with First Row Transition Metal Complexes. *Chem. Rev.* **2019**, *119* (4), 2752−2875.

(2) Zhang, B.; Sun, L. Artificial Photosynthesis: Opportunities and Challenges of Molecular Catalysts. *Chem. Soc. Rev.* **2019**, *48* (7), 2216−2264.

(3) Leung, J. J.; Warnan, J.; Ly, K. H.; Heidary, N.; Nam, D. H.; Kuehnel, M. F.; Reisner, E. Solar-Driven Reduction of Aqueous CO2 with a Cobalt Bis(Terpyridine)-Based Photocathode. *Nat. Catal.* **2019**, *2* (4), 354−365.

(4) Roy, S.; Miller, M.; Warnan, J.; Leung, J. J.; Sahm, C. D.; Reisner, E. Electrocatalytic and Solar-Driven Reduction of Aqueous CO_2 with Molecular Cobalt Phthalocyanine−Metal Oxide Hybrid Materials. *ACS Catal.* **2021**, *11* (3), 1868−1876.

(5) Schreier, M.; Gao, P.; Mayer, M. T.; Luo, J.; Moehl, T.; Nazeeruddin, M. K.; Tilley, S. D.; Grätzel, M. Efficient and Selective Carbon Dioxide Reduction on Low Cost Protected Cu_2O Photocathodes Using a Molecular Catalyst. *Energy Environ. Sci.* **2015**, *8* (3), 855−861.

(6) Schreier, M.; Luo, J.; Gao, P.; Moehl, T.; Mayer, M. T.; Grätzel, M. Covalent Immobilization of a Molecular Catalyst on Cu_2O Photocathodes for CO_2 Reduction. *J. Am. Chem. Soc.* **2016**, *138* (6), 1938−1946.

(7) Pati, P. B.; Wang, R.; Boutin, E.; Diring, S.; Jobic, S.; Barreau, N.; Odobel, F.; Robert, M. Photocathode Functionalized with a Molecular Cobalt Catalyst for Selective Carbon Dioxide Reduction in Water. *Nat. Commun.* **2020**, *11* (1), 3499.

(8) Liu, J.; Shi, H.; Shen, Q.; Guo, C.; Zhao, G. Efficiently Photoelectrocatalyze CO_2 to Methanol Using Ru(II)-Pyridyl Complex Covalently Bonded on TiO_2 Nanotube Arrays. *Applied Catalysis B: Environmental* **2017**, *210*, 368−378.

(9) Koida, T.; Fujiwara, H.; Kondo, M. Hydrogen-Doped In_2O_3 as High-Mobility Transparent Conductive Oxide. *Jpn. J. Appl. Phys.* **2007**, *46* (No. 28), L685−L687.

(10) Calnan, S.; Tiwari, A. N. High Mobility Transparent Conducting Oxides for Thin Film Solar Cells. *Thin Solid Films* **2010**, *518* (7), 1839−1849.

(11) Powalla, M.; Paetel, S.; Ahlswede, E.; Wuerz, R.; Wessendorf, C. D.; Magorian Friedlmeier, T. Thin-film Solar Cells Exceeding 22% Solar Cell Efficiency: An Overview on CdTe-, $Cu(In,Ga)Se_2$ -, and Perovskite-Based Materials. *Appl. Phys. Rev.* **2018**, *5* (4), No. 041602.

(12) Lee, T. D.; Ebong, A. U. A Review of Thin Film Solar Cell Technologies and Challenges. *Renew. Sust. Energy Rev.* **2017**, *70*, 1286−1297.

(13) Green, M. A.; Dunlop, E. D.; Siefer, G.; Yoshita, M.; Kopidakis, N.; Bothe, K.; Hao, X. Solar Cell Efficiency Tables (Version 61). *Progress in Photovoltaics* **2023**, *31* (1), 3−16.

(14) Jehl, Z.; Rousset, J.; Donsanti, F.; Renou, G.; Naghavi, N.; Lincot, D. Electrodeposition of ZnO Nanorod Arrays on ZnO Substrate with Tunable Orientation and Optical Properties. *Nanotechnology* **2010**, *21* (39), No. 395603.

(15) Haller, S.; Suguira, T.; Lincot, D.; Yoshida, T. Design of a Hierarchical Structure of ZnO by Electrochemistry for ZnO-Based Dye-Sensitized Solar Cells: Design of a Hierarchical Structure of ZnO by Electrochemistry. *Phys. Stat. Sol. (a)* **2010**, *207* (10), 2252−2257.

(16) Peulon, S.; Lincot, D. Mechanistic Study of Cathodic Elecfrodeposition of Zinc Oxide and Zinc Hydroxychioride Films from Oxygenated Aqueous Zinc Chloride Solutions. *J. Electrochem. Soc.* **1998**, *145* (3), 864−874.

(17) Gallanti, S.; Chassaing, E.; Lincot, D.; Naghavi, N. Influence of Thiourea Addition on the Electrodeposition of ZnO from Zinc Nitrate Aqueous Solutions. *Electrochim. Acta* **2015**, *178*, 225−233.

(18) Lincot, D. Solution Growth of Functional Zinc Oxide Films and Nanostructures. *MRS Bull.* **2010**, *35* (10), 778−789.

(19) Manzano, C. V.; Philippe, L.; Serrà, A. Recent progress in the electrochemical deposition of ZnO nanowires: synthesis approaches and applications. *Crit. Rev. Solid State Mater. Sci.* **2022**, *47*, 772−805.

(20) Guerrero, J.; Schneider, N.; Dumoulin, F.; Lincot, D.; Isci, U.; Naghavi, N.; Robert, M. Transparent Porous ZnO|Metal Complex Nanostructured Materials: Application to Electrocatalytic CO2 Reduction. *ACS Appl. Nano. Mater.* **2023**, *6*, 10626−10635.

(21) Yoshida, T.; Zhang, J.; Komatsu, D.; Sawatani, S.; Minoura, H.; Pauporté, T.; Lincot, D.; Oekermann, T.; Schlettwein, D.; Tada, H.; Wöhrle, D.; Funabiki, K.; Matsui, M.; Miura, H.; Yanagi, H. Electrodeposition of Inorganic/Organic Hybrid Thin Films. *Adv. Funct. Mater.* **2009**, *19* (1), 17−43.

(22) Liu, Y.; Xia, M.; Ren, D.; Nussbaum, S.; Yum, J.-H.; Grätzel, M.; Guijarro, N.; Sivula, K. Photoelectrochemical CO_2 Reduction at a Direct $CuInGaS_2$ /Electrolyte Junction. *ACS Energy Lett.* **2023**, *8*, 1645−1651.

(23) Costentin, C.; Robert, M.; Savéant, J.-M. Catalysis of the Electrochemical Reduction of Carbon Dioxide. *Chem. Soc. Rev.* **2013**, *42* (6), 2423−2436.

(24) Costentin, C.; Drouet, S.; Passard, G.; Robert, M.; Savéant, J.-M. Proton-coupled electron transfer cleavage of heavy-atom bonds in electrocatalytic processes. Cleavage of a C-O bond in catalyzed electrochemical reduction of CO_2. *J. Am. Chem. Soc.* **2013**, *135* (24), 9023−9031.

(25) Boutin, E.; Merakeb, L.; Ma, B.; Boudy, B.; Wang, M.; Bonin, J.; Anxolabéhère-Mallart, E.; Robert, M. Molecular catalysis of CO_2 reduction. Some recent advances and perspectives in electrochemical and light-driven processes with Fe, Ni and Co aza macrocyclic and polypyridine complexes. *Chem. Soc. Rev.* **2020**, *49*, 5772−5809.

(26) Guillén, E.; Peter, L. M.; Anta, J. A. Electron Transport and Recombination in ZnO-Based Dye-Sensitized Solar Cells. *J. Phys. Chem. C* **2011**, *115* (45), 22622−22632.

https://doi.org/10.1021/acsenergylett.3c01205
ACS Energy Lett. 2023, 8, 3488−3493